Analysis and Control of Equivalent Physical Simulator for Nanosatellite Space Radiator

Yun-Ze Li, *Member, IEEE*, Kok-Meng Lee, *Fellow, IEEE*, and Jun Wang

***Abstract*—A realistic prediction of the in-orbit transient performance of a nanosatellite space radiator requires a ground-based equivalent space radiator with a small size, simple configuration, and fast response. For this purpose, we present in this paper the design concept, operating principle, and analysis algorithm of a novel equivalent physical simulator (EPS) consisting of a thermoelectric cooler (TEC), a plate-fin heat sink, and a forced cooling fan. The TEC-based EPS achieves the purpose of simulating the in-orbit transient heat radiation in earth's atmospheric environment by adapting two key parameters: the TEC cooling capacity and the thermal resistance of the heat sink cooling fan. This paper offers results of in-depth numerical parametric studies leading to an EPS design that enables robust simulations under both hot-case and cold-case operations. In addition, we present the design and evaluation of a fuzzy controller for the EPS as an attractive alternative to the traditional PID controller. The fuzzy control presented here will have other potential thermal control applications where TECs and forced cooling heat sinks are employed.**

***Index Terms*—Fuzzy control, ground-based physical simulation, nanosatellite, space radiator, thermoelectric cooler.**

I. Introduction

RECENT advances in the microelectromechanical systems fabrication technology with increased computing power, along with the interest to reduce size, power consumption, and fabrication cost, have resulted in a number of emerging mechatronics. Among these are nanosatellites (each with a wet mass between 1 and 10 kg or 2.2–22 lb) that have the potential of revolutionizing the space industry and help achieve ambitious missions, such as interspacecraft communications [1], earth observation [2], and space investigation related to solar science, atmospheric, magnetospheric, astrophysics, and interplanetary environment [1]. Space radiators play an important role in dissipating heat generated inside the satellite to the space environment [3]; the transfer process is dominated by the heat radiation at the radiator surface [4]–[7]. Because of their large power density and small available surface area for radiation, nanosatellites are subject to a relatively stiff heat-dissipating task. In addition, the thermal capacity of nanosatellites is typically smaller than that of traditional satellites. However, the effects of external heat flux (such as direct solar radiation, earth IR, and earth-reflected solar radiation) on the transient thermal response of radiators and on the internal temperature dynamics of a nanosatellite are much more than those of large ones. These, combined with highly integrated systems that dissipate large amounts of power in a small volume, demand a careful designing of the thermal control system to meet the stringent temperature control requirements.

Space simulators are essential tools for predicting the thermal performance of the satellite surfaces, which include radiators [8]. A typical space simulator usually consists of a vacuum chamber, heat sink, cryogenic subsystem, heating subsystem, and vacuum-pumping subsystem [9]–[11]. This ground-based physical simulation approach has been widely used in the thermal cycling, vacuum, and balance tests [12]–[14] for a satellite. However, these traditional space simulators are too large, complex, and slow for investigating the dynamics of the internal thermal control loop strategies of the nanosatellite or the effects of an active thermal control, where critical response time requirements must be met.

To alleviate this problem, a smaller and simpler (but with a faster response) ground-based physical apparatus, referred to here as an equivalent physical simulator (EPS), is required as a rational basis for simulating the nanosatellite space radiator (nS-SR), and for investigating the dynamic performance of its internal thermal control system. Thermoelectric coolers (TECs), which are much more compact than other kinds of refrigerators, are among the best candidates for the EPS, because of their small size, low thermal inertia, fast dynamic response, and ease of control. Although the TEC has been widely employed in the thermal management of electronic systems where extremely stable temperature control is required, most of the studies have largely focused on the design, analysis, and experiment of thermoelectric elements [15]–[20]. Due to the highly nonlinear dynamic behavior of the thermoelectric module [21], it is quite difficult to model its transient performance accurately with theoretical equations; thus, a linear approximation is often rendered to simplify it for a control system design. A practical alternative to this perturbation control system analysis is the employment of fuzzy logics, which has shown some potential to improve the control effect of the thermoelectric system [22]. Similar improvements can also be found in other fuzzy applications such as the robotic tracking of moving objects [23], robot navigation [24], gas turbine control [25], and more recently, mechatronic system modeling [26]. However, unlike the traditional TEC applications where the cold-side temperature is

Manuscript received November 30, 2008; revised February 9, 2009. First published April 17,2009; current version published November 18, 2009. Recommended by Technical Editor G. Yang. This work was supported by the National Natural Science Foundation of China under Grant 50506003.

Y.-Z. Li and J. Wang are with the School of Aeronautic Science and Engineering, Beihang University, Beijing 100191, China (e-mail: liyunze@ buaa.edu.cn; wangjun@ buaa.edu.cn).

K.-M. Lee is with the George W. Woodruff School of Mechanical Engineering, Georgia Institute of Technology, Atlanta, GA 30332-0405 USA (e-mail: kokmeng.lee@me.gatech.edu).

Color versions of one or more of the figures in this paper are available online at http://ieeexplore.ieee.org.

Digital Object Identifier 10.1109/TMECH.2009.2016957

usually the only controlled variable and is always lower than the surrounding temperature [15]–[22], the desired cold-side working temperature of the TEC for the ground-based space radiator EPS may be *higher than*, *lower than,* or *equal to* the atmospheric temperature. In addition, the cooling heat flux and cold-side temperature of the TEC during the transient in earth's convection environment must be controlled with high precision to simulate those of the space radiation heat transfer. These differences demand special design considerations and advanced control strategies to meet stringent requirements, including a wide working range and high simulating precision of the ground-based EPS.

The remainder of this paper offers the following.

1) We present the design concept and working principle of a novel EPS developed for an nS-SR. The EPS consisting of a TEC and a fan/sink cooling system simulates the heat-dissipating effect of the nS-SR by adjusting the TEC cooling capacity under an intelligent fuzzy control. The TEC-based EPS is conveniently small and structurally simple, but sufficiently fast in dynamic response for a ground-based experimental investigation of the transient performance impact on the internal thermal control system of the nS-SR being tested.
2) Along with the description of an analysis algorithm for design parametric studies, we numerically simulate the effects of two key parameters (the coefficient of performance of the TEC and the thermal resistance of the cooling system) on the hot-side temperature, EPS power supply, and robustness to thermal load changes. These analytical investigations not only help gain intuitive insights into design tradeoffs, but also provide a basis to develop essential criteria for design optimization of an effective EPS.
3) We offer an intelligent fuzzy control approach for controlling the TEC and its hot-side working temperature, and numerically evaluate its control performances (subject to step disturbances due to thermal load changes and air temperature variation) against those under the traditional PID control. As will be shown, the response of the fuzzy-controlled EPS agrees well with that of the simulated nS-SR. In addition, it offers a faster response and exhibits a smaller overshoot than that under the PID control.

II. Design Concept, Principle, and Analysis

The nS-SR is a special component on the outer surface of the nanosatellite, which has the characteristics of high emittance and low absorptance. The nS-SR is connected to the internal heat sources of the nanosatellite through devices or materials (such as a heat pipe or graphite) [1] that have a low thermal resistance to heat transfer. The function of the nS-SR is to dissipate heat generated inside the satellite to the space environment, as shown in Fig. 1, where $T_{\rm r}$ is the temperature at the radiator surface (with area A). When flying in a low earth orbit, the nS alternates between the shadow of earth and the direct exposure of sunlight. In the orbit, the transfer process at the outer surface of the nS-SR is dominated by the heat radiation [Fig. 1(a)] with the net

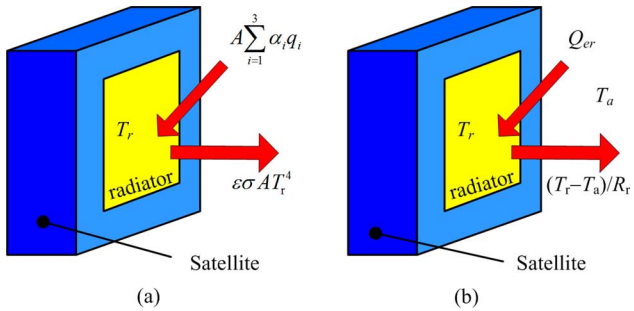

Fig. 1. Heat transfer of a nanosatellite space radiator. (a) In-orbit. (b) In-earth-atmosphere.

radiant heat flux given by

$$Q_{\rm r} = \varepsilon\sigma A T_{\rm r}^4 - A\sum_{i=1}^{3}\alpha_i q_i \tag{1}$$

where σ is the Stefan–Boltzmann constant; ε is the radiator surface emittance; α_i and q_i are the radiator absorptance and radiant heat flux density at the outer surface, respectively; and the subscripts $i = 1$–3 denote the contributions from the solar radiation, earth radiation, and albedo (or the earth surface reflectivity of sun radiation), respectively.

Before the nanosatellite is launched into its orbit, the heat dissipation is governed by heat convection between the radiator and earth's atmosphere [Fig. 1(b)] with the net convective heat flux expressed as

$$Q_{\rm r} = Q_{\rm er} - (T_{\rm r} - T_{\rm a})/R_{\rm r},\ \text{where}\ R_{\rm r} = 1/(h_{\rm r}A_{\rm r}) \tag{2}$$

where $Q_{\rm er}$ is total external radiation heat flux absorbed by the nS-SR; $T_{\rm a}$ is the atmosphere temperature; and $R_{\rm r}$ and $h_{\rm r}$ are the thermal resistance and the heat transfer coefficient between the outer surface of the nS-SR and its surrounding air (usually in the form of natural heat convection.), respectively.

The need to simulate the space radiation heat transfer (1) under the heat transfer mode (2) in earth's convection environment makes it necessary to develop a ground-based simulator that can experimentally investigate the static temperature distribution and transient temperature response of the nanosatellite, so that its in-orbit thermal control effects are well understood, especially during the design and development phase, and the evaluation testing stage of a new satellite.

A. EPS of the nS-SR

Fig. 2 shows the EPS for realistically simulating the thermal behavior of the nS-SR on ground. The primary components of the EPS are the TEC and the plate-fin heat sink with a forced cooling fan. The sensors used in the EPS feedback-controlled system include a heat flux sensor (denoted as $Q_{\rm c}$ in Fig. 2) mounted on the cold side of the TEC and two temperature sensors (denoted in Fig. 2 as $T_{\rm h}$ and $T_{\rm c}$, respectively) placed on the hot and cold sides of the TEC.

When the EPS is employed for ground-based experiments, the cold side of the TEC is attached to the nS-SR surface, and the other surfaces of the nanosatellite are covered with thermal

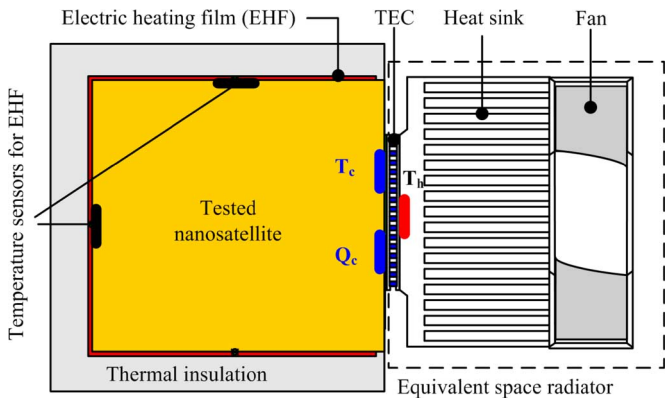

Fig. 2 EPS.

insulation, so that the influence of earth's atmosphere on their thermal states can be minimized. To simulate the effect of the external heating phenomenon on the other surfaces of the nanosatellite, electric heating films (with a set of temperature sensors) are placed on the inside of this thermal insulation layer.

As illustrated in Fig. 2, the EPS (TEC, heat sink, cooling fan, and thermal insulation) is an external system (not a part of the nanosatellite in-orbit), which acts as a ground-based equivalent space radiator to physically produce simulated cooling effects and similar temperature boundary conditions of an in-orbit nS-SR.

In operation, the electric current input to the TEC is adjusted according to the cooling heat flux and temperature (Q_c and T_c) on the cold side of the TEC to simulate the cooling effect of the nS-SR equivalently. Since the *real* temperature T_r (of the nS-SR being simulated) may be higher or lower than earth's atmospheric temperature T_a, a flexible controller for the hot-side temperature T_h must be designed, so that both cold case ($T_r < T_a$) and hot case ($T_r \geq T_a$) can be simulated. This means that the thermal resistance of the heat sink must be adjusted according to the cold-side temperature T_c. This is realized by manipulating the electric current that drives the forced cooling fan.

B. Governing Equations

To illustrate the operational principle, we treat the cold side of the TEC as a lumped-parameter node in modeling the EPS dynamics

$$(V_c \rho_c c_c)\,\dot{T}_c = Q_i - Q_c \tag{3}$$

where (V_c, ρ_c, c_c) are the volume, average density, and specific heat of the TEC; T_c and Q_i are the temperature and the thermal load on the cold side of the TEC; and Q_c is the TEC cooling capacity. The theoretical cooling capacity of the TEC for a specified electric current I_t passing through it is given by (3a)

$$Q_c = \alpha_t T_c I_t - R I_t^2/2 - K\,(T_h - T_c) \tag{3a}$$

where α_t, R, and K are the Seeback coefficient, electrical resistance, and thermal conductivity of the TEC, respectively; and T_h is the hot-side temperature of the TEC.

To simulate the in-orbit thermal behavior of the nS-SR equivalently using the TEC, the cooling capacity Q_c and the cold-side temperature T_c of the TEC should be equal to the net radiant heat flux Q_r and the working temperature T_r of the nS-SR, respectively; in other words,

$$Q_c \to Q_r \text{ at } T_c \to T_r = \text{specified working temperature.} \tag{3b}$$

The desired condition (3b) is accomplished by adjusting the electric current I_t of the TEC to reach the equivalent cooling effect. Since (3a) and (3b) must be met simultaneously, the electric current to drive the TEC for simulating the in-orbit heat radiation can be found by equating them

$$I_t = \frac{1}{R}\left(\alpha_t T_c \pm \sqrt{\alpha_t^2 T_c^2 - 2RQ_e}\right) \tag{4}$$

where

$$Q_e = \varepsilon\sigma A T_c^4 - A\sum_{i=1}^{3}\alpha_i q_i + K(T_h - T_c). \tag{4a}$$

The lower value of the solution of (4) is preferred to reduce the TEC power consumption *P*, which is given by

$$P = \alpha_t(T_h - T_c)I_t + I_t^2 R. \tag{5}$$

Similarly, we treat the TEC hot side and the heat sink together as another lumped-parameter node, and neglect the small thermal resistance between the TEC and the heat sink. The total heat flux Q_h (including Q_c and *P* consumed by the TEC) reaching the hot side of the TEC must be rejected to earth's atmosphere (at temperature T_a) through the heat sink. The cooling fan offers a means to manipulate the thermal resistance R_h between the hot side of the TEC and earth's atmosphere by adjusting its electric current I_f. Thus, the EPS dynamics on the hot side is given by (6)

$$(V_h \rho_h c_h)\,\dot{T}_h = Q_h - (T_h - T_a)/R_h \tag{6}$$

where (V_h, ρ_h, c_h) are the volume, density, and specific heat of the heat sink. The heat flux Q_h $(= Q_c + P)$ pumped to the TEC hot side can be calculated from

$$Q_h = \alpha_t T_h I_t + R I_t^2/2 - K(T_h - T_c). \tag{6a}$$

The desired thermal resistance R_h of the heat sink, which is defined in (6b), is determined from the forced convection at the heat sink surface

$$R_h = \frac{T_h - T_a}{Q_h} = \left(\frac{1}{\dot{m}c_{pa}}\right)\frac{\exp(\gamma)}{\exp(\gamma) - 1},$$
$$\text{where} \quad \gamma = \eta\frac{h_h A_h}{\dot{m}c_{pa}} \tag{6b}$$

where γ is the number of transfer units of the heat sink; $(\dot{m}, c_{pa})$ are the mass flow rate and specific heat of the forced cooling air; A_h, h_h are the heat transfer area and convective heat transfer coefficient between the heat sink surface and air. In (6b), the fin efficiency η depends on the geometric parameters and cooling conditions of the heat sink; methods for calculating the fin efficiency can be found in [16].

Given the cooling capacity Q_c in (3a) and power supply P in (5), the TEC performance can be evaluated using the parameter coefficient of performance (COP) defined in (7)

$$\mathrm{COP} = Q_c/P. \tag{7}$$

A high COP means less power consumed by the TEC, the key component in simulating the nS-SR.

C. Design Analysis Algorithm

A key step in the EPS design analysis is to determine the hot-side temperature T_h, which is a function of the thermal resistance of the heat sink in (6b) and the power consumed by the TEC in (5), at the simulated cooling condition. An iteration algorithm (based on the secant method) has been developed to compute the hot-side temperature T_h with an initial $T_{h,0}$ value

$$T_{h,k+1} = T_{h,k} - \frac{f(I_{t,k}, T_{h,k})}{f(I_{t,k}, T_{h,k}) - f(I_{t,k-1}, T_{h,k-1})}(T_{h,k} - T_{h,k-1}) \tag{8}$$

where

$$T_{h,0} = \max(T_c, T_a). \tag{8a}$$

In (8), the subscript "k" denotes the kth iteration in the computation; and I_t is given in (4). The final T_h for the iterative computation is reached when

$$T_{h,k+1} - T_{h,k} \le e_{\min} \tag{8b}$$

where $e_{\min}$ is a specified error tolerance.

For the specified Q_c and T_c determined by the cooling effect and working temperature of the simulated nS-SR, the calculation of the hot-side temperature T_h can be based on one of the two design parameters; namely, the specified COP of the TEC or the desired thermal resistance R_h of the heat sink.

1) COP defined in (7) is selected as the design parameter

$$f(I_{t,k}, T_{h,k}) = Q_{c,k} - (\mathrm{COP})P_k \tag{9a}$$

where Q_c and P are given in (3a) and (5).

2) R_h defined in (6b) is selected as the design parameter

$$f(I_{t,k}, T_{h,k}) = Q_{h,k} - (T_{h,k} - T_a)/R_h \tag{9b}$$

where Q_h is given in (6a).

As an illustration, we numerically investigate the effects of the two design parameters, COP and R_h, on the required hot-side working temperature T_h and the power supply P of the EPS, which developed during the transient thermal performance experiment of a 10-W nanosatellite. The values of the physical parameters used in the analysis are summarized in Table I. Since the radiator is almost in earth's shadow and the radiator absorptions α_i are usually quite small, the absorbed radiant heat flux ($\alpha_i q_i$) on the outer surface is considered negligible as compared to the dominating T_c^4 term in (4a). The computed results illustrating the effects of COP (from 0.1 to 10) and R_h (0.1–1.25 K/W) are plotted in Figs. 3 and 4, respectively. Some observations in Figs. 3 and 4 are briefly discussed as follows.

TABLE I
VALUES OF EPS PARAMETERS

Parameter (Unit)	Symbol	Value
Design specification		
Cooling capacity (W)	Q_c	10
Cold-side temperature (K)	T_c	300
Atmospheric temperature (K)	T_a	298.15 (25°C)
TEC parameters		
Seeback coefficient (W/K/A)	α_t	0.051
Electrical resistance (Ω)	R	2.22
Thermal conductivity (W/K)	K	0.5808
Specific heat (kg/m^3)	ρ_c	2420
Average density (kJ/kg)	c_c	0.713
Geometrical dimension (mm)	H×L×W	4.5×40×40
Plate-fin Heat Sink		
Device dimension (mm)	H×L×W	34×82×67.5
Specific heat (kg/m^3)	ρ_h	2610
Average density (kJ/kg)	c_h	0.904
Fin height, length, thickness, space (mm)	h_f, l_f, w_f, w_s	30, 82, 1.0, 2.5
Number of fins	N	20

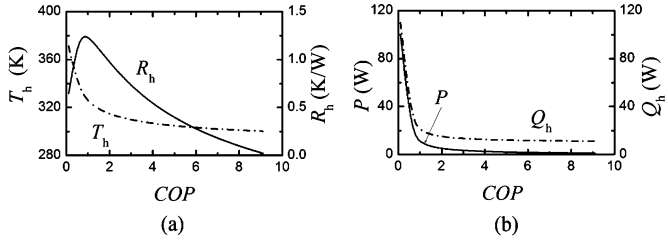

Fig. 3. Effect of COP.

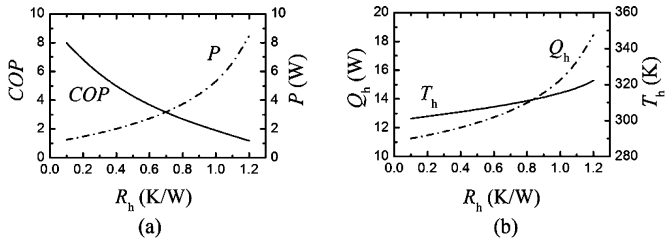

Fig. 4. Effect of R_h.

1) Fig. 3(a) shows that for a very small COP, T_h decreases rapidly, while R_h increases and reaches its maximum of 1.3 K/W (at COP ≈0.75), beyond which R_h decreases gradually as T_h continues to drop, but very slowly, to its final value of about 300.5 K. Both P and Q_h drop as COP increases [Fig. 3(b)] until COP ≈1.0, beyond which both decrease very slowly.
2) The relationship between COP and R_h can also be observed in Fig. 4(a). The electric power supply P increases as a result of a decreasing COP, while Q_h increases, as shown in Fig. 4(b); more heat needs to be dissipated to the environment causing an increase in the hot-side temperature, T_h.
3) The aforesaid observations suggest that to make the TEC work more efficiently, the COP should be higher than 1.0, T_h and R_h should be as low as possible to minimize the electrical power P consumed by the TEC and the heat Q_h

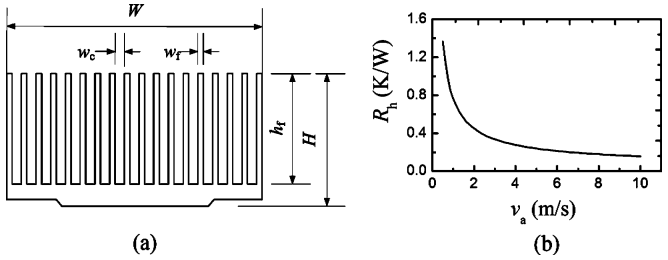

Fig. 5. Plate-fin heat sink and its thermal resistance. (a) Heat sink dimensions. (b) Thermal resistance variation.

to be dissipated by the heat sink/fan to the atmosphere. However, a decrease in the thermal resistance $R_{\rm h}$ would demand a higher air velocity, and hence, more power is consumed by the cooling fan. This phenomenon implies a power consumption tradeoff (in terms of $R_{\rm h}$) between the TEC and the cooling fan. Fig. 5(a) shows an example of a plate-fin heat sink for the TEC, which offers a tradeoff between high COP and low thermal resistance, $R_{\rm h}$. The geometrical parameters and thermal properties of the heat sink are given in Table I. As graphed in Fig. 5(b), $R_{\rm h}$ varies from 0.1 to 1.4 K/W as the average velocity $v_{\rm a}$ of the forced cooling air (flowing inside heat sink channel) changes from 0.1 to 10 m/s. The corresponding Reynolds number ranges from 144.5 to 2890.

D. Robustness to Variable State Performance

The procedure in Section II-C illustrates the design of the EPS for a specified cooling capacity and cold-side temperature. The EPS must be capable of robustly and efficiently simulating the space thermal behavior under other thermal working conditions as characterized by (1) that relates the net radiant heat flux $Q_{\rm r}$ with the simulated nS-SR temperature $T_{\rm r}$. When the thermal load of the tested nanosatellite changes, the TEC cold-side temperature $T_{\rm c}$ and cooling capacity $Q_{\rm c}$ must adapt accordingly to the physical simulation law given by (3b). The change in the working performance of the nS-SR is referred to here as the "variable state performance."

The following two case operations are required as part of the TEC-based EPS simulation:

$$\text{Cold case } (T_{\rm r} < T_{\rm a}) \text{ and hot case } (T_{\rm r} \geq T_{\rm a}).$$

However, for equivalent ground-based experiments, the TEC hot-side temperature $T_{\rm h}$ must be higher than earth's atmospheric temperature $T_{\rm a}$ to allow heat dissipation, and as low as possible for the economical operation of the TEC. To accommodate these requirements, the hot-side temperature $T_{\rm h}$ of the TEC is adapted using the control strategy (10)

$$T_{\rm h} = \begin{cases} T_{\rm a} + \delta_{\rm c}, & \text{if } T_{\rm r} < T_{\rm a} \text{ (cold-case)} \\ T_{\rm c} + \delta_{\rm h}, & \text{if } T_{\rm r} \geq T_{\rm a} \text{ (hot-case)} \end{cases} \tag{10}$$

where $\delta_{\rm c}$ and $\delta_{\rm h}$ are small positive constants for the efficient operation of the TEC and the ease of control of the cooling fan.

For both cold- and hot-case simulations, $T_{\rm h}$ is manipulated by adjusting the electric current to the cooling fan, as discussed

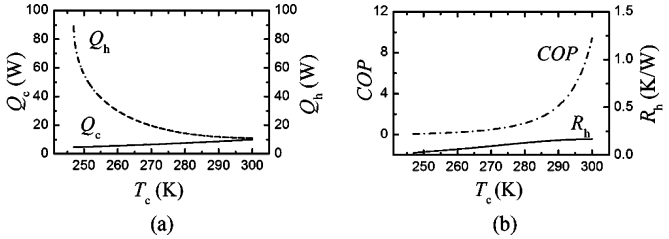

Fig. 6. Cold-case ($T_{\rm c} < T_{\rm a}$) variable state performance. (a) Heat fluxes at two sides of TEC. (b) COP and thermal resistance.

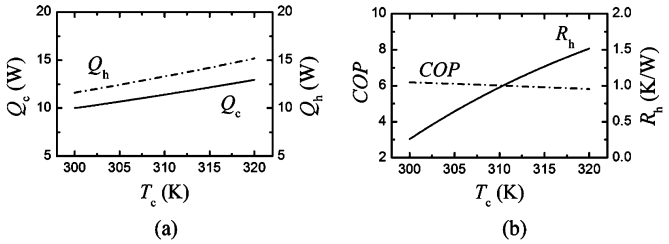

Fig. 7. Hot-case ($T_{\rm c} \geq T_{\rm a}$) variable state performance. (a) Heat fluxes at two sides of TEC. (b) COP and thermal resistance.

in previous sections. The variable state performance of the EPS can be analyzed by using the following algorithmic steps.

Step 1: Determine $Q_{\rm c}$ based on (1) and (3b), and set $T_{\rm r} = T_{\rm c}$.

Step 2: Calculate $T_{\rm h}$ using (10).

Step 3: Compute $I_{\rm t}$, P, and $Q_{\rm h}$ of the TEC for the given $Q_{\rm c}, T_{\rm c}$, and $T_{\rm h}$ using (4), (5), and (6a), respectively.

Step 4: Once $T_{\rm h}$ and $Q_{\rm h}$ are known for a given $T_{\rm a}$, the required value of $R_{\rm h}$ can be obtained using its definition, (6b).

Step 5: Evaluate the TEC performance using the parameter COP, which can be calculated from (7).

To illustrate the effectiveness of the $T_{\rm h}$ adaptation, we analyze the variable state performance of the same design (as discussed in Section II-C, where the design for the nominal load of $Q_{\rm c} =$ 10 W at $T_{\rm c} = 300$ K and $T_{\rm a} = 25\,^{\circ}$C are summarized in Table I) for the following operations:

$$\text{Cold case } (245 \text{ K} < T_{\rm c} < 300 \text{ K}), \qquad \delta_{\rm c} = 2.85 \text{ K}$$

$$\text{Hot case } (300 \text{ K} \leq T_{\rm c} < 320 \text{ K}), \qquad \delta_{\rm h} = 3 \text{ K}.$$

Since $\delta_{\rm c}$ and $\delta_{\rm h}$ are constants, $T_{\rm h}$ can be determined from (10) for given $T_{\rm a}$ and $T_{\rm c}$. Only the changes in $Q_{\rm c}, Q_{\rm h}, R_{\rm h}$, and COP are graphed in Figs. 6 and 7 for the cold- and hot-case operations, respectively. Figs. 6 and 7 are discussed as follows.

1) Figs. 6(a) and 7(a) show that the cooling capacity $Q_{\rm c}$ increases with $T_{\rm c}$ as expected in (1), which describes the simulated thermal performance of the nS-SR.
2) Under the cold-case operation, where $T_{\rm c}$ decreases below the nominal (or design) temperature of $T_{\rm c} = 300$ K, $Q_{\rm h}$ increases rapidly due to a dramatic decrease in the COP, as shown in Fig. 6(a) and (b). Fig. 6(b) also indicates only a slight decrease in the required $R_{\rm h}$ as $T_{\rm c}$ decreases because $T_{\rm h}$ remains unchanged while $Q_{\rm h}$ increases.
3) On the other hand, both $Q_{\rm h}$ and $Q_{\rm c}$ increase gradually (approximately at the same rate) under the hot-case

operation, where T_c increases above the nominal 300 K, as shown in Fig. 7(a); this is because with the T_h adaptation, $T_h - T_c = \delta_h = 3$ K, a constant. It is worth noting that when $T_c > T_a, T_h$ must increase such that it is always higher than T_c; otherwise, the TEC would not work properly. For T_c to rise from 300 to 320 K, R_h must increase from 0.5 to 1.5 K/W [Fig. 7(b)], so that the EPS can simulate a cooling temperature higher than T_a.

4) The COP exhibits two different trends as evident from a comparison between Figs. 6(b) and 7(b). As T_c increases, the COP rises dramatically when $T_c < T_a$, but drops slightly when $T_c \geq T_a$. The reason for this difference is that the TEC temperature increment $(T_h - T_c)$ decreases for the cold case, but does not change for the hot case based on the operating policy (10).

III. EPS Dynamics and Control System

The TEC as well as the forced cooling fan with the heat sink of the EPS are typical nonlinear controlled systems. There are difficulties in reducing their nonlinear constitutive equations to simple linear models, and yet accurately and conveniently reflecting their dynamics [19]. Also, there are challenges of experimentally identifying the parameters that characterize the linear dynamical model under various working conditions [21]. To overcome these difficulties, we explore here a fuzzy control algorithm as an effective alternative to traditional control methods [22], [23].

A. Intelligent Controller

Fig. 8(a) and(b) shows the block diagram illustrating the EPS control system and the fuzzy logic controller. The hardware implementing the intelligent controller is illustrated in Fig. 8(c), where two sensors measuring T_c and heat flux Q_c are mounted on the cold side, and another temperature sensor is placed on the hot side of the TEC. The sensing signals are fed to the integrated control unit as inputs. The control unit outputs two signals manipulating the electric currents that drive the TEC and the cooling fan of the heat sink.

As shown in Fig. 8(a), the cold-side cooling heat flux Q_c and the hot-side temperature T_h are manipulated through the electrical currents (I_t and I_f) to the TEC and the cooling fan, respectively. The corresponding reference values are given by the following converting functions:

$$Q_{cr} = \varepsilon\sigma A T_c^4 - Q_{er} \tag{11}$$

and

$$T_{hr} = \max(T_c, T_a) + \delta \tag{12}$$

where Q_{er} is the total external space heat flux absorbed by the simulated nS-SR. In (12), δ is a small constant (usually about 1–5K) and is added to maintain a positive $(T_h - T_a)$ under the cold case or a positive $(T_h - T_c)$ under the hot case, so that heat can be transferred out of the heat sink or the TEC, respectively.

Fig. 8(b) shows the fuzzy incremental controller consisting of a fuzzifier, an inference engine, a defuzzifier, and a fuzzy rule base. The inputs to the fuzzifier are the error e_n and its difference e_{cn} normalized by the factors K_e and K_c. Similarly, the output u_{cn} (scaled by the factor, K_u) leaving the defuzzifier is a normalized increment of the controlling variable u (I_f or I_c). The input and output variables to the fuzzy controller are characterized by the fuzzy sets, linguistic values, and associated analytical ranks shown in Table II. Each fuzzy set (or its linguistic value) is defined by a Gaussian membership function shown in Fig. 9. The membership functions have an overlap with each other to provide a smooth output transition between the regions.

The controller output is determined using the linguistic rules in the following form:

$$\text{IF } e_n \text{ is } E_i \text{ and } e_{cn} \text{ is } CE_j, \text{ THEN } u_{cn} \text{ is } CU_{\ell(i,j)}$$

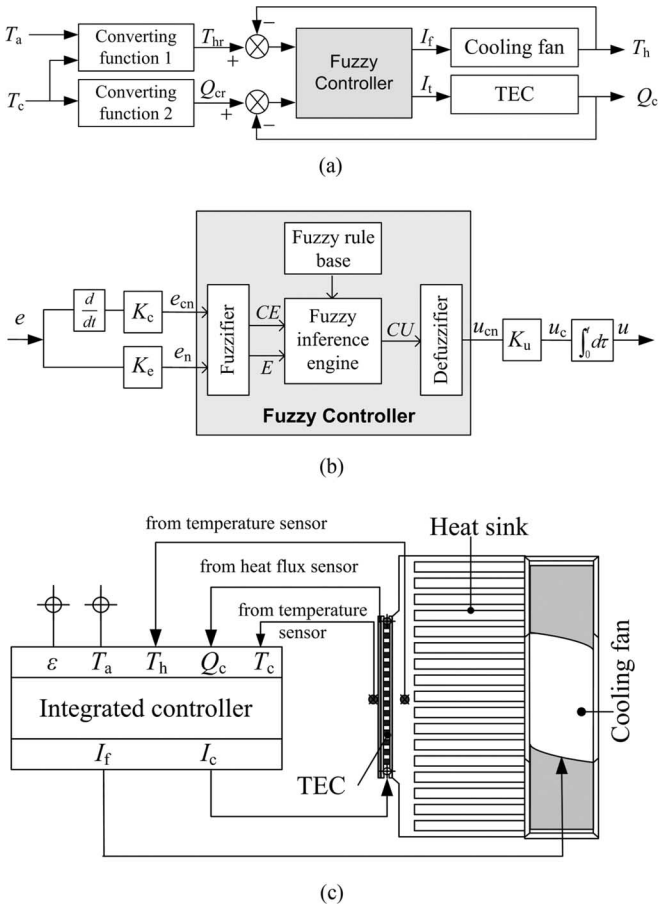

Fig. 8. Block diagrams illustrating the EPS controller. (a) Control block diagram. (b) Fuzzy control system components. (c) EPS control system configuration.

TABLE II
Fuzzy Sets and Their Linguistic Values

Fuzzy sets	Ranks*	Linguistic values	Fuzzy sets	Ranks*	Linguistic values
NS	–4	negative super	PS	4	positive super
NH	–3	negative high	PH	3	positive high
NM	–2	negative medium	PM	2	positive medium
NL	–1	negative low	PL	1	positive low
ZE	0	zero			

* Associated ranks are for the convenience of producing rules defined by (13).

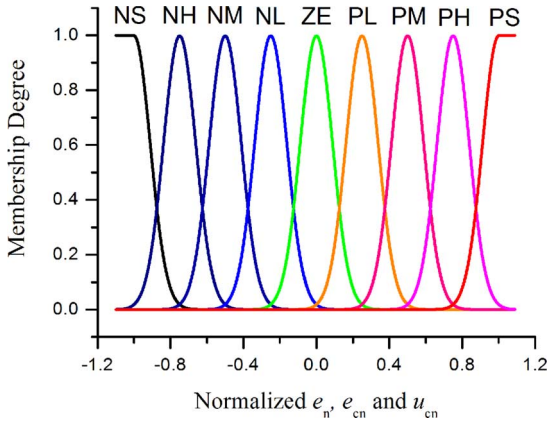

Fig. 9. Membership functions.

where E_i, CE_j, and $CU_{\ell(i,j)}$ are the fuzzy values of $e_{\rm n}, e_{\rm cn}$, and $u_{\rm cn}$; and the subscript variables i, j, and $\ell(i,j)$ denote the analytical ranks associated with these linguistic values, as shown in Table II. For a two-input system ($e_{\rm n}$ and $e_{\rm cn}$, each with nine fuzzy values), a fully populated rule base will have $9 \times 9 = 81$ input rule combinations derived with the help of simulations, which suggests the following.

1) A positive error $e_{\rm n}$ can be effectively reduced by a positive input increment to the TEC, but a negative input increment to the cooling fan.
2) When the error $e_{\rm n}$ is positively large but its difference $e_{\rm cn}$ is negatively large, the input increments should be zero or negatively low to the TEC, and zero or positively low to the cooling fan, because a reverse error change rate can effectively reduce the control output changes to achieve a better result.
3) Similarly, when $e_{\rm n}$ is negatively large but $e_{\rm cn}$ is positively large, the input increments to the TEC should be zero or positively low, and to the cooling fan should be zero or negatively low.

On the basis of these insights, the rank-based rule-generating policy is derived in (13)

$$\ell(i,j) = \begin{cases} +\left[\varphi i + (1-\varphi) j\right], & \text{TEC control} \\ -[\varphi i + (1-\varphi) j], & \text{fan control.} \end{cases} \tag{13}$$

where φ is the error impact power determined by the rank of the input error. Here, the same parameter producing law is used for both TEC control and its fan control

$$\varphi = 0.8 - 0.1\,|i|\,, \qquad \text{where } 0 \le i \le 4. \tag{14}$$

Fuzzy control rules produced by (13) and (14) for the intelligent control of the TEC and heat sink cooling fan are plotted in Fig. 10, which are rounded off to integer ranks for characterizing into a nine-element fuzzy set {NS, NH, NM, NL, ZE, PL, PM, PH, PS}. As the control rules [Fig. 10(b)] for the cooling fan are complements of those for the TEC [Fig. 10(a)], only the fuzzy control rules of the TEC intelligent controller are summarized in Table III.

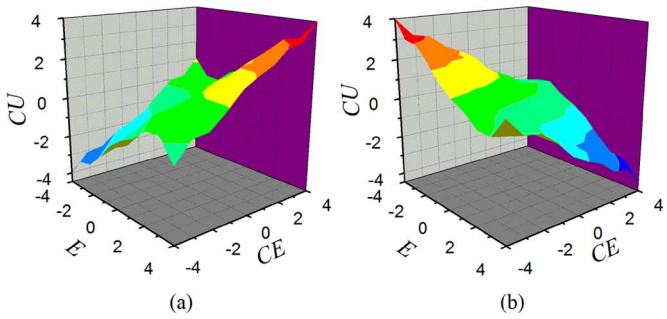

Fig. 10. Surface map of the fuzzy control rule base. (a) TEC control. (b) Forced cooling fan control.

TABLE III
FUZZY CONTROL RULES OF TEC

E_i/CE_i	NS	NH	NM	NL	ZE	PL	PM	PH	PS
NS	NS	NH	NH	NM	NM	NL	ZE	ZE	PL
NH	NH	NH	NM	NM	NL	NL	ZE	ZE	ZE
NM	NH	NM	NM	NM	NL	NL	ZE	ZE	ZE
NL	NM	NM	NL	NL	NL	ZE	ZE	ZE	PL
ZE	NL	NL	ZE	ZE	ZE	ZE	ZE	PL	PL
PL	NL	ZE	ZE	ZE	PL	PL	PL	PM	PM
PM	ZE	ZE	ZE	PL	PL	PM	PM	PM	PH
PH	ZE	ZE	ZE	PL	PL	PM	PM	PH	PH
PS	NL	ZE	ZE	PL	PM	PM	PH	PH	PS

In Fig. 8(b), the output from the defuzzifier takes the following form:

$$u_{\rm cn} = \frac{\sum_{i=1}^{9}\sum_{j=1}^{9} u_{{\rm cn},\ell(i,j)}\lambda_{\ell(i,j)}}{\sum_{i=1}^{9}\sum_{j=1}^{9}\lambda_{\ell(i,j)}} \tag{15}$$

where $u_{{\rm cn},\ell(i,j)}$ and $\lambda_{\ell(i,j)}$ are the representative discrete element and membership degree of the output fuzzy set, $CU_{\ell(i,j)}$. The next control step u' can then be determined in terms of the current control step u and $u_{\rm cn}$ by (16)

$$u' = u + K_{\rm u} u_{\rm cn}, \qquad \text{where} \qquad u \in \{I_{\rm t}, I_{\rm f}\}\,. \tag{16}$$

B. Simulation of the Dynamics and Control

To examine the effectiveness of the fuzzy-controlled EPS, we predict its dynamics subject to disturbances due to the following:

1) a -5 K step change in the atmospheric temperature $T_{\rm a}$;
2) a $+10\%$ step change in the input thermal load $Q_{\rm i}$.

As a basis for evaluation, we compare the predictions against the simulations of a PID-controlled EPS system (with parameters $K_{\rm p}, K_{\rm p}/T_{\rm i}, K_{\rm p}T_{\rm d}/T_{\rm s}$, where $K_{\rm p}$ is a proportional gain; $T_{\rm i}$ and $T_{\rm d}$ are the integral and derivative times in seconds, respectively; and $T_{\rm s}$ is the sampling period). The values of the parameters used in the simulation are summarized in Table IV.

The effectiveness of the fuzzy controller (Fig. 8), along with the $T_{\rm h}$ adaptation strategy (10), can be observed from the simulated transient responses of the cold- and hot-side temperatures ($T_{\rm c}$ and $T_{\rm h}$) given in Figs. 11–13.

1) As shown in Fig. 11(a), in response to the -5 K step change in the surrounding atmosphere, $T_{\rm r}$ remains unchanged as expected in (1), since there is no change in

TABLE IV
PARAMETERS OF SIMULATED CONTROLLERS

Fuzzy controller			PID controller		
Parameters	TEC	Fan	Parameters	TEC	Fan
K_e	0.05	0.01	K_p	0.055	–0.05
K_c	0.05	0.01	T_i	10	15
K_u	1.0	1.0	T_d	0.05	0
Sampling period, T_s=1.0 second					

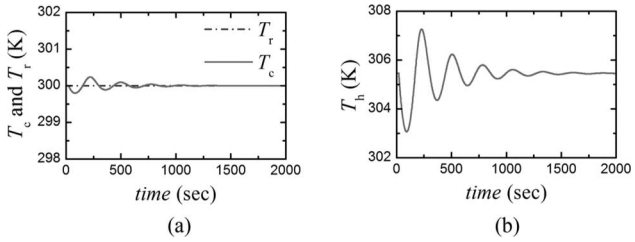

Fig. 11. Effect of -5 K change in T_a on fuzzy-controlled EPS. (a) Cold-side temperature. (b) Hot-side temperature.

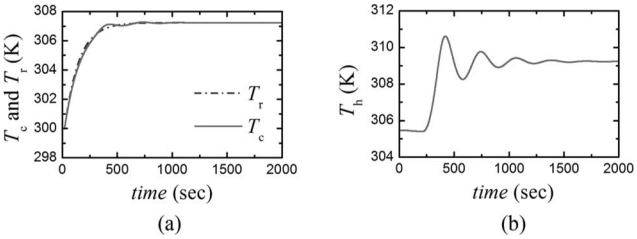

Fig. 12. Effect of $+10\%$ step change in Q_i on fuzzy-controlled EPS. (a) Cold-side temperature. (b) Hot-side temperature.

the input cooling load, and in orbit, T_a does not affect the simulated nS-SR temperature; T_c fluctuates within 2% of its steady state value (the absolute overshoot is only 0.25 K and agrees with T_r well). The effect of the -5 K step change in T_a can be seen in Fig. 11(b) to be primarily taken on by T_h during this transient, which returns to its steady-state value after a few oscillations (but no more than ± 2 K).

2) Fig. 12(a) compares the transient responses of the cold-side temperature T_c and the simulated nS-SR temperature T_r to a $+10\%$ change in Q_i. The simulation shows that T_c and T_r settle to the new steadystate value of 307 K in approximately 320 s with little or no significant overshoot. The transient responses of T_c and T_r closely agree with each other; the dynamic tracking error of T_c with respect to T_r is less than 0.25 K. The corresponding transient response of the hot-side temperature T_h is given in Fig. 11(b). Unlike the cold-side temperature, T_h exhibits a 35% overshoot (about 1.4 K) and a pure time delay by 230 s because of the thermal inertia of heat sink, as shown in (3). This overshoot and delay, however, are acceptable since they do not affect the T_c response.
3) As compared in Fig. 13, the fuzzy-controlled T_c and T_r are more responsive and with a smaller overshoot than that of a PID control when experiencing a $+10\%$ step change in Q_i.

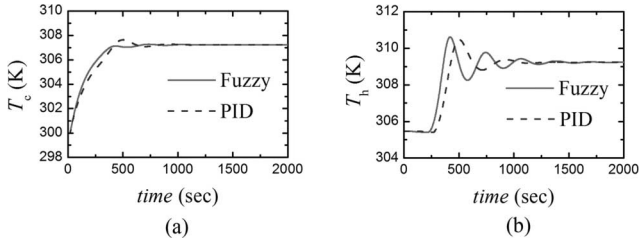

Fig. 13. Comparison between Fuzzy and PID EPS control ($+10\%$ change in Q_i). (a) Cold-side temperature. (b) Hot-side temperature.

IV. CONCLUSION

We have presented the design concept, principle, and analysis of a ground-based EPS for simulating the transient heat radiation of an in-orbit nS-SR in earth's atmospheric environment. The TEC-based EPS achieves this purpose by adapting the TEC cooling capacity and the thermal resistance of the heat sink cooling fan. The fuzzy control strategies aimed at achieving effective and robust physical simulation performance have been detailed.

Numerical analyses for design parametric studies and for investigating the robustness of the variable state performance have been illustrated. Specifically, we identify two key design parameters (the COP of the TEC and the desired thermal resistance of the heat sink cooling fan), and analyze the tradeoffs between them. We also offer the method of adapting the hot-side temperature of the TEC, which enables robust EPS simulations under both hot-case and cold-case operations. In addition, we present the design of the fuzzy-controlled EPS and evaluate its performance by comparing the transient temperature responses of the ground-based EPS and the real in-orbit nS-SR to a step change in thermal load. The results demonstrate that the fuzzy controller with the method of hot-side temperature adaptation is an attractive alternative to the traditional PID controller.

While the intelligent fuzzy logic control discussed here has been illustrated in the context of a simple and intelligent EPS (which greatly facilitates the testing of nanosatellites before they are launched), it is expected that the method would have potential applications in other thermal control systems where TECs and forced cooling heat sinks are employed.

ACKNOWLEDGMENT

The authors would like to thank Prof. Y.-H. Li for his suggestions and contributions to this paper. This study was partly carried out during Y.-Z. Li's stay at Georgia Institute of Technology.

REFERENCES

[1] P. V. Panetta, "NASA-GSFC nano-satellite technology development," *Proc. AIAA/USU Conf. Small Satellites*, 1998, pp. 1–17.
[2] J. Esper, P. V. Panetta, M. Ryschkewithsch, W. Wiscombe, and S. Neeck, "NASA-GSFC nano-satellite technology for earth science missions," *Acta Astronaut.*, vol. 46, no. 2–6, pp. 287–296, 2000.

[3] V. Baturkin, "Micro-satellites thermal control concept and components," *Acta Astronaut.*, vol. 56, no. 1–2, pp. 161–170, 2005.
[4] R. Osiander, S. L. Firebaugh, J. L Champion, D. Farrar, and M. A. G. Darrin, "Microelectromechanical devices for satellite thermal control," *IEEE Sensors J.*, vol. 4, no. 4, pp. 525–531, Aug. 2004.
[5] W. Biter, S. Hess, O. Sung, D. Douglas, and T. Swanson, "Electrostatic radiator for satellite temperature control," in *Proc. IEEE Aerosp. Conf.*, 2005, pp. 781–790.
[6] D. Farrar, W. Schneider, R. Osiander, J. L. Champion, A. G. Damn, D. Douglas, and T. D. Swamon, "Controlling Variable Emittance (MEMS) Coatings for space applications," in *Proc. Intersoc. Conf. Therm. Thermomech. Phenom. Electron. Syst.*, pp. 1020–1024.
[7] D. G. Gilmore, *Spacecraft Thermal Control Handbook*, 2nd ed. vol. 1, Segundo, CA: The Aerospace Press, 2002, pp. 21–67, 709–757.
[8] R. D. Stark, "Thermal testing of spacecraft," The Aerospace Corp., Los Angeles, CA, Rep. TOR-0172(2441-01)-4, Sep. 1971.
[9] *Test Requirements for Launch, Upper Stage, and Space Vehicles,* Department of Defense Handbook, vol. 1 and 2, MIL-STD-340 A (USAF), Apr. 1999.
[10] *Product Verification Requirements for Launch, Upper Stage, and Space Vehicles,* Department of Defense Standard Practice, MIL-STD-1540D, Jan. 1999.
[11] M. K. Choi, "Thermal design of Landsat-7 ETM Earth/space background simulators," in *Proc. IECEC 1997 Energy Convers. Eng. Conf. (IECEC)*, vol. 2, pp. 1470–1475.
[12] R. O. Ambrose and R. S. Askew, "An experimental investigation of actuators for space robots," in *Proc. IEEE Int. Conf. Robot. Autom.*, 1995, vol. 3, pp. 2625–2630.
[13] W. J. Krotiuk, "Engineering testing of the capillary pumped loop thermal control system for the NASA EOS-AM spacecraft," in *Proc. IECEC 1997*, vol. 2, pp. 1463–1469.
[14] T. W. Kerslake, L. S. Mason, and H. J. Strumpf, "High-flux, high-temperature thermal vacuum qualification testing of a solar receiver aperture shield," in *Proc. IECEC 1997*, vol. 1, pp. 440–445.
[15] D. M. Rowe, *CRC Handbook of Thermoelectrics*. New York: CRC Press, 1995, ch. 55.
[16] A. Bejan, *Heat Transfer Handbook*. Hoboken, NJ: Wiley, 2003, pp. 1029–1131.
[17] B. J. Huang, C. J. Chin, and C. L. Duang, "A design method of thermoelectric cooler," *Int. J. Refrig*, vol. 23, pp. 208–218, 2000.
[18] R. Chein and Y. Chen, "Performances of thermoelectric cooler integrated with microchannel heat sinks," *Int. J. Refrig.*, vol. 28, pp. 828–839, 2005.
[19] M. Anatone and R. Cipollone, "Theoretical and experimental analysis on thermoelectric cooling devices," *J. Thermophys. Heat Transfer*, vol. 15, no. 4, pp. 447–452, 2001.
[20] L. U. Odhner and H. H. Asada, "Sensorless temperature estimation and control of shape memory alloy actuators using thermoelectric devices," *IEEE/ASME Trans. Mechatronics*, vol. 11, no. 2, pp. 139–144, Apr. 2006.
[21] B. J. Huang and C. L. Duang, "System dynamic model and temperature control of a thermoelectric cooler," *Int. J. Refrig.*, vol. 23, pp. 197–207, 2000.
[22] A. A. Aly and E. A. S. Abo, "Fuzzy temperature control of a thermoelectric cooler," in *Proc. IEEE Int. Conf. Ind. Technol.*, 2006, pp. 1580–1585.
[23] K.-M. Lee and Y. Qian, "A vision-guided fuzzy logic control system for dynamic pursuit of moving target," *Microprocess. Microsyst.*, vol. 21, pp. 571–580, 1998.
[24] X. Chen, K. Watanabe, K. Kiguchi, and K. Izumi, "An ART-based fuzzy controller for the adaptive navigation of a quadruped robot," *IEEE/ASME Trans. Mechatronics*, vol. 7, no. 3, pp. 318–328, Sep. 2002.
[25] J.-W. Kim and S. W. Kim, "Design of incremental fuzzy PI controllers for a gas-turbine plant," *IEEE/ASME Trans. Mechatronics*, vol. 8, no. 3, pp. 410–414, Sep. 2003.
[26] K. Erenturk, "Hybrid control of a mechatronic system: Fuzzy logic and grey system modeling approach," *IEEE/ASME Trans. Mechatronics*, vol. 12, no. 6, pp. 703–710, Dec. 2007.

Yun-Ze Li (M'09) received the B.S. degree in thermal and electrical engineering from the Northern China Institute of Water Conservancy and Electric Power, Zhengzhou, China, in 1996, the M.S. degree in thermal power engineering from Xi'an Jiaotong University, Xi'an, China, in 2000, and the Ph.D. degree in engineering thermal physics from Tsinghua University, Beijing, China, in 2002.

He has been an Associate Professor in the School of Aeronautic Science and Engineering, Beihang University, Beijing, since 2004. He was an Assistant Engineer with Xingtai Power Corporation, Hebei, China, from 1996 to 1997, and a Postdoctoral Researcher at Beijing University of Aeronautics and Astronautics, Beijing, from 2003 to 2004. In 2007, he was a Visiting Scholar at Georgia Institute of Technology, Atlanta, and at National Cheng-Kung University, Tainan, Taiwan, in 2008. His current research interests include thermal control, energy management, and environmental control of aerospace systems.

Kok-Meng Lee (M'89–SM'02–F'05) received the B.S. degree from the State University of New York, Buffalo, in 1980, and the S.M. and Ph.D. degrees from Massachusetts Institute of Technology, Cambridge, in 1982 and 1985, respectively.

Currently, he is a Professor in the Woodruff School of Mechanical Engineering, Georgia Institute of Technology, Atlanta. His current research interests include system dynamics/control, robotics, automation, and mechatronics. He holds eight patents in machine vision, 3-DOF spherical motor/encoders, and live-bird handling system.

Prof. Lee is a Fellow of the American Society of Mechanical Engineers (ASME). He received the National Science Foundation (NSF) Presidential Young Investigator, Sigma Xi Junior Faculty Research, International Hall of Fame New Technology, and Kayamori Best Paper Awards.

Jun Wang received the B.S. degree in aerospace engineering from Beijing University of Aeronautics and Astronautics, Beijing, China, in 1959.

He is currently a Professor in the School of Aeronautic Science and Engineering, Beihang University, Beijing. His current research interests include environmental control and simulation of aerospace system, air conditioning, and refrigeration.

Prof. Wang has been a member of the Chinese Academy of Engineering since 2001. He is the Chairman of the Science and Technology Association of Beihang University. Also, he is the Administrative Syndic and a Senior Member of the Chinese Association of Refrigeration.